



HAL
open science

Theoretical gas and dielectric second virial coefficients of CO-Ar

Antonio Rizzo, Javier Lopez Cacheiro, Berta Fernandez Rodriguez, Branislav
Jansik, Thomas Bondo Pedersen

► **To cite this version:**

Antonio Rizzo, Javier Lopez Cacheiro, Berta Fernandez Rodriguez, Branislav Jansik, Thomas Bondo Pedersen. Theoretical gas and dielectric second virial coefficients of CO-Ar. *Molecular Physics*, 2008, 106 (07), pp.881-892. 10.1080/00268970802001363 . hal-00513183

HAL Id: hal-00513183

<https://hal.science/hal-00513183>

Submitted on 1 Sep 2010

HAL is a multi-disciplinary open access archive for the deposit and dissemination of scientific research documents, whether they are published or not. The documents may come from teaching and research institutions in France or abroad, or from public or private research centers.

L'archive ouverte pluridisciplinaire **HAL**, est destinée au dépôt et à la diffusion de documents scientifiques de niveau recherche, publiés ou non, émanant des établissements d'enseignement et de recherche français ou étrangers, des laboratoires publics ou privés.



Theoretical gas and dielectric second virial coefficients of CO-Ar

Journal:	<i>Molecular Physics</i>
Manuscript ID:	TMPH-2007-0384.R1
Manuscript Type:	Full Paper
Date Submitted by the Author:	18-Feb-2008
Complete List of Authors:	Rizzo, Antonio; IPCF, CNR, Pisa, Italy Lopez Cacheiro, Javier; University of Santiago de Compostela, Faculty of Chemistry, Chemistry Fernandez Rodriguez, Berta; University of Santiago de Compostela, Faculty of Chemistry, Chemistry Jansik, Branislav; Aarhus Universitet, Teoretisk Kemi Bondo Pedersen, Thomas; University of Lund, Theoretical Chemistry
Keywords:	Interaction Induced electric polarizability, van der Waals complex, dielectric virial coefficients, gas virial coefficient, Interaction Induced electric dipole
<p>Note: The following files were submitted by the author for peer review, but cannot be converted to PDF. You must view these files (e.g. movies) online.</p> <p>TMPH-2007-0384_Revised.tex</p>	



1
2
3
4
5
6
7
8
9
10
11
12
13
14
15
16
17
18
19
20
21
22
23
24
25
26
27
28
29
30
31
32
33
34
35
36
37
38
39
40
41
42
43
44
45
46
47
48
49
50
51
52
53
54
55
56
57
58
59
60

For Peer Review Only

1
2
3
4
5
6
7
8
9
10
11
12
13
14
15
16
17
18
19
20
21
22
23
24
25
26
27
28
29
30
31
32
33
34
35
36
37
38
39
40
41
42
43

Theoretical pressure and dielectric second virial coefficients of CO-Ar

Javier López Cacheiro*, Berta Fernández

*Department of Physical Chemistry, Faculty of Chemistry,
University of Santiago de Compostela,
E-15782 Santiago de Compostela, Spain*

Antonio Rizzo

*Istituto per i Processi Chimico-Fisici del Consiglio Nazionale delle Ricerche,
Area della Ricerca, via G. Moruzzi 1,
loc. S. Cataldo, I-56124 Pisa, Italy*

Branislav Jansík

*Teoretisk Kemi, Kemisk Institut,
Aarhus Universitet,
Langelandsgade 140,
8000 Aarhus C, Denmark*

Thomas Bondo Pedersen†

*Department of Theoretical Chemistry,
Chemical Center, University of Lund,
P.O. Box 124, S-221 00 Lund, Sweden*

* Present Address: CESGA. Avenida de Vigo s/n Campus Sur, E-15705 Santiago de Compostela, Spain

† Present Address: Atomistix A/S, c/o Niels Bohr Institute, Rockefeller Complex, Juliane Maries Vej 30, DK-2100 Copenhagen, Denmark

Abstract

Using coupled cluster singles and doubles linear response theory and the d-aug-cc-pVTZ basis set extended with a $3s3p2d1f1g$ set of midbond functions, the interaction induced electric dipole polarizability surface of the CO-Ar van der Waals complex is computed. Combining this surface with accurate intermolecular potential energy and electric dipole surfaces, the pressure and dielectric second virial coefficients of the complex are calculated by a classical statistical approach. Excellent agreement with experimental results (to within the experimental error bars) is obtained for the pressure second virial coefficient over a range of temperatures. No previous experimental or theoretical investigations have been carried out for the dielectric second virial coefficient, $B_\epsilon(T)$, which is estimated to be about $1.9 \text{ cm}^6 \text{ mol}^{-1}$ at room temperature. This value results from a balance of terms due to the interaction induced electric dipole polarizability (predominant at high temperatures) and orientational electric dipole contributions.

I. INTRODUCTION

The CO-Ar complex is a well studied van der Waals system, see e.g. Ref. 1 for a recent review of experimental and theoretical work on its intermolecular rovibrational structure. Owing to its small size, the highly precise experimental data are matched by the high degree of accuracy achievable with the most sophisticated *ab initio* approaches available in concurrent quantum chemistry software packages.

Previously, we have computed the rovibrational spectrum of CO-Ar^{2,3} as well as modelled the Ar broadening of CO absorption lines.⁴ In Ref. 2 we evaluated rovibrational energies from a three-dimensional *ab initio* intermolecular potential energy surface calculated with the size-extensive coupled cluster singles and doubles (CCSD)⁵ including connected triples (CCSD(T))⁶ model and the augmented correlation consistent polarized valence quadruple zeta (aug-cc-pVQZ)^{7,8} basis set extended with a $3s3p2d1f1g$ (denoted 33211 in the following) set of midbond functions.⁹ Approximately a thousand experimentally assigned rovibrational transitions were reproduced with a root-mean-square error of 0.13 cm^{-1} , excluding states observed in the region around 25 cm^{-1} above the ground state, where much larger discrepancies with respect to the experimental results were found.

In order to shed light on these differences, we subsequently studied³ the temperature-dependent spectral intensities computed from a CCSD/aug-cc-pVTZ-33211 interaction induced dipole surface and suggested an alternative assignment of the experimental lines. Controversy still remains, however, and Havenith and Schwaab¹ have recently proposed a new semi-empirical potential energy surface which preserves the original assignments of experimental lines. This surface differs from all previous theoretical and semi-empirical ones in that it contains a local minimum at the linear Ar—CO ($\theta = 180^\circ$) geometry.

In the present work we proceed along this line of studies and evaluate an accurate electric dipole polarizability surface to help in characterizing the CO-Ar interaction. We use the d-aug-cc-pVTZ-33211 basis set and CCSD linear response theory for computing the surface from which, in turn, we evaluate the dielectric second virial coefficient using a classical statistical averaging procedure.

Interaction induced polarizabilities are well known to be a source of information on intermolecular forces, and therefore a lot of work has been carried out over the last years

1
2
3 aimed mainly at their accurate experimental determination.^{10–15} From the theoretical
4 point of view the evaluation of interaction induced polarizabilities in van der Waals com-
5 plexes is a challenge. The dispersion character of the van der Waals interaction places
6 substantial demands on the level of electron correlation treatment and on the choice of the
7 basis set. In previous work, we have carried out accurate studies of interatomic potentials
8 and of various interaction induced electric properties and second virial coefficients for the
9 dielectric constant and refractivity, the electric second harmonic generation (ESHG) hy-
10 perpolarizability, and the Kerr constant of the helium, neon, and argon homonuclear^{16–23}
11 as well as heteronuclear^{24,25} van der Waals dimers. In all cases the interaction poten-
12 tials and the interaction induced properties were computed at the CCSD(T) and CCSD
13 levels of theory, respectively. For evaluating the second virial coefficients we have used
14 both semiclassical and quantum statistical approaches, and the general conclusion is that
15 quantum corrections are negligible except at very low temperatures. In addition, quan-
16 tum statistical corrections are in general a quite formidable task for systems involving
17 more than two atoms. In this work we therefore disregard quantum statistical effects
18 altogether.

19
20
21 Dielectric second virial coefficient measurements in mixtures involving $\text{CF}_3\text{H}-\text{Ar}$ and
22 CFH_3-Ar have been presented quite some years ago by Sutter and Cole,²⁶ who used
23 a novel technique developed in collaboration with Buckingham.²⁷ Copeland and Cole
24 later reproduced with good accuracy the results of measurements employing a theoretical
25 model of pair interactions.²⁸ These properties are difficult to obtain, as proven by our
26 previous work where it was found that in some cases revision of experimental data is
27 needed.²¹ No previous experimental or theoretical investigations of the dielectric second
28 virial coefficient of $\text{CO}-\text{Ar}$ have been reported, and we hope that the present results may
29 serve as a motivation for future studies.

30 31 32 33 34 35 36 37 38 39 40 41 42 43 44 45 46 47 48 49 50 51 52 53 54 55 56 57 58 59 60

II. DEFINITIONS AND COMPUTATIONAL DETAILS

For the system investigated here, the dielectric second virial coefficient $B_e(T)$ is given,
within a semiclassical approach, as a sum of two distinct contributions:^{25,28,29} an in-
duced moment effect $B_e(\text{ind})$ and an orientational contribution $B_e(\text{or})$. The former is ob-
tained by integration of the isotropic interaction induced polarizability $\Delta\alpha_{ave}(r, R, \theta) =$

$[\Delta\alpha_{xx}(r, R, \theta) + \Delta\alpha_{yy}(r, R, \theta) + \Delta\alpha_{zz}(r, R, \theta)]/3$, a function of the CO internuclear distance r , the distance between the center of nuclear masses of carbon monoxide and the argon atom R , and of the angle θ made by the axis of CO and the z -axis, aligned along the line connecting the center of nuclear masses of CO to the atom (i.e. $\theta = 0^\circ$ and $\theta = 180^\circ$ correspond to linear CO—Ar and Ar—CO, respectively), according to

$$B_\epsilon(\text{ind}) = \frac{\pi N_A^2}{3\epsilon_0} \int \Delta\alpha_{ave}(r, R, \theta) \exp\left[-\frac{\Delta V(r, R, \theta)}{kT}\right] R^2 dR \sin\theta d\theta = \frac{N_A^2}{6\epsilon_0} X[T, r, I[\Delta\alpha]], \quad (1)$$

whereas the orientation contribution is calculated as

$$B_\epsilon(\text{or}) = \frac{\pi N_A^2}{9\epsilon_0 kT} \int [\mu^2(r, R, \theta) - \mu_{\text{CO}}^2(r)] \exp\left[-\frac{\Delta V(r, R, \theta)}{kT}\right] R^2 dR \sin\theta d\theta. \quad (2)$$

Above $\Delta V(r, R, \theta)$ is the interaction potential, k the Boltzmann constant, N_A Avogadro's number, ϵ_0 the vacuum permittivity and T the temperature. We employ the notation

$$X[T, r, I[P]] = 2\pi \int I[P](T, r, R, \theta) dR d\theta, \quad (3)$$

$\mu(r, R, \theta)$ is the dipole moment of the van der Waals complex, which in Ref. 3 was written as

$$\mu_z(r, R, \theta) = \mu_{\text{CO}}(r) \cos\theta + \Delta\mu_z(r, R, \theta) \quad (4)$$

$$\mu_x(r, R, \theta) = \mu_{\text{CO}}(r) \sin\theta + \Delta\mu_x(r, R, \theta) \quad (5)$$

in terms of the interaction induced dipole moment $\Delta\mu(r, R, \theta)$ and of the dipole moment of carbon monoxide $\mu_{\text{CO}}(r)$ (complex on the x, z plane). Therefore

$$B_\epsilon(\text{or}) \approx \frac{N_A^2}{18\epsilon_0 kT} X[T, r, I[\Delta\mu^2]] + \frac{N_A^2}{9\epsilon_0 kT} \mu_{\text{CO}}(r) X[T, r, I[\Delta\mu]] \quad (6)$$

$$= B_\epsilon^{(\Delta\mu^2)}(\text{or}) + B_\epsilon^{(\Delta\mu)}(\text{or}) \quad (7)$$

$$X[T, r, I[\Delta\mu^2]] = 2\pi \int \Delta\mu^2(r, R, \theta) \exp\left[-\frac{\Delta V(r, R, \theta)}{kT}\right] R^2 dR \sin\theta d\theta \quad (8)$$

$$X[T, r, I[\Delta\mu]] = 2\pi \int [\Delta\mu_z(r, R, \theta) \cos\theta + \Delta\mu_x(r, R, \theta) \sin\theta] \exp\left[-\frac{\Delta V(r, R, \theta)}{kT}\right] R^2 dR \sin\theta d\theta \quad (9)$$

Throughout the present work the CO internuclear distance is kept fixed at the experimentally determined equilibrium value $r = 1.128206 \text{ \AA}$.³⁰ Keeping the CO distance fixed provides a significant computational simplification by reducing the number of points to

be computed in the induced electric dipole polarizability surface and by reducing the dimensionality of the classical integration from six to two variables. The contribution to the electric properties due to the vibrational structure of the CO molecule is thus neglected. This approximation can be employed without sacrificing accuracy: it was shown in Ref. 2 that vibrational contributions (from CO) are negligible for the potential surface of the trimer, except at very short CO–Ar distances. Since the static dipole moment and polarizability are derivatives of this surface with respect to the electric field strength, it is reasonable to assume that vibrational contributions are negligible for these quantities as well.

The CCSD(T)/aug-cc-pVQZ-33211 interaction potential discussed in Ref. 2 is employed. The CCSD/aug-cc-pVTZ-33211 interaction induced dipole moment given in Ref. 3 corresponding to the equilibrium value of r was originally obtained for a rather limited range of Ar-CO distances, and the functional form obtained in Ref. 3 was found to be poorly suited for the long range extrapolations needed to perform the integrations of Eqs. 8 and 9. Indeed it was found that for a large range of angles θ the parallel component extrapolated from the functional form of Ref. 3 diverges as R increases above ≈ 12 -13 au. For this reason we have extended the number of points of the interaction induced dipole moment surface computed with respect to those of Ref. 3. A total of 325 points were computed, for the equilibrium value of r , in a range of R from 2.75 Å to 20 Å. The same wave function model and basis set exploited in Ref. 3 were employed. The induced dipole moment was recomputed with a geometrical setup corresponding to a rotation by $\pi/2 - \theta$ with respect to the one adopted here, see above, and which corresponds to an arrangement where the CO molecule is aligned along the x' axis. The complete set of results is available in Ref. 31. We label the computed induced electric dipole moment as $\Delta\mu'(R, \theta)$. The relationships

$$\Delta\mu_z(r, R, \theta) = \Delta\mu'_x(r, R, \theta) \cos \theta + \Delta\mu'_z(r, R, \theta) \sin \theta \quad (10)$$

$$\Delta\mu_x(r, R, \theta) = \Delta\mu'_x(r, R, \theta) \sin \theta - \Delta\mu'_z(r, R, \theta) \cos \theta \quad (11)$$

trivially hold.

The two components $\Delta\mu'_x(R, \theta)$ and $\Delta\mu'_z(R, \theta)$ (at $r = 1.128206$ Å) were then fitted

to the functional forms (R in Å and θ in radians, electric dipole in au)

$$\Delta\mu'_x(R, \theta) = \sum_{\lambda=1}^{10} \sum_{\rho=1}^5 C_{\lambda\rho}^x R^{-D_\rho^x} \theta^\lambda, \quad (12)$$

$$\Delta\mu'_z(R, \theta) = \sum_{\lambda=0}^9 \sum_{\rho=1}^5 C_{\lambda\rho}^z R^{-D_\rho^z} \theta^\lambda, \quad (13)$$

which yield an excellent smooth analytical description of the behavior of the interaction dipole surface, and they are employed — after transformation according to Eqs. 10 and 11 — in the calculation of the integrals of Eqs. 8 and 9. The parameters $C_{\lambda\rho}^\sigma$ and D_ρ^σ ($\sigma=x,z$) are given in Table I. The high quality of the fit within the range of values for R and θ where the property was computed analytically was checked carefully, and it can be appreciated by an inspection of Fig. 1, which shows both the *ab initio* computed points and the interpolating curve for a selection of R distances as a function of the angle θ . The long range behavior appears to be well reproduced, and the analytical form was employed far beyond the region of interpolation, see below for a discussion of the techniques of integration. The experimental dipole moment of CO (at $r = 1.128206$ Å, $\mu_{\text{CO}}(r) = +0.0481131$ e a_0 , corresponding to a relative electric polarity $-\text{CO}+$)³² was employed for the purpose of evaluating the $B_\epsilon^{(\Delta\mu)}$ (or) contribution.

The interaction induced electric dipole polarizability was computed at several intermolecular geometries chosen so that the range of values for R and θ where the integrand of Eq. 1 is non-negligible is reasonably covered. For this purpose, we use CCSD linear response theory as implemented in the DALTON program³³ and the d-aug-cc-pVTZ-33211 basis set. The latter was chosen after a series of test calculations at the intermolecular equilibrium geometry $R = 3.73$ Å, $\theta = 93^\circ$,² carried out using the *x*aug-cc-pVXZ ($x = -, d, t$; $X = T, Q$) basis sets. The Boys-Bernardi counterpoise correction³⁴ is employed to account for basis set superposition errors. A subset of the computed interaction induced electric dipole polarizabilities is given in Table II. The whole set of values, which were computed for a finer grid of values of θ than shown in the Table (a total of 210 points) is available in Ref. 31.

The calculated interaction induced electric dipole polarizabilities are fitted to the function (again R in Å and θ in radians, yielding polarizability in au),

$$\Delta\alpha_{ave}(R, \theta) = \sum_{\lambda=0}^{\mathcal{N}} \left[\sum_{n=0}^{\mathcal{N}} C_{\lambda n} R^n \right] \exp(-D_\lambda R) P_\lambda(\theta), \quad (14)$$

where $P_\lambda(\theta)$ denotes the Legendre polynomial of order λ . Different values of \mathcal{N} were used to find the optimal size of the expansion. The expansion with $\mathcal{N} = 6$ contains 56 parameters and has enough flexibility to yield a smooth description of the property; the resulting parameters are given in Table III. In spite of its formal appearance, which might lead to suspect that the competition of large powers of R and exponential decay in the expansion may at some point yield a wrong long range behavior, Eq. 14 performs indeed remarkably well very far beyond the range of internuclear distances employed in our semiclassical integration. The excellent agreement between computed *ab initio* property and interpolating function is shown in Fig. 2, where the interpolating function Eq. 14 is plotted for the series of values of R corresponding to those of Table II, ranging from 2.75 Å up to 20.0 Å, as θ varies from 0° to 180° . In Fig. 2 also the computed values of the interaction induced electric dipole polarizability are shown. The maximum errors of the interpolation amount to a few percent only, with larger deviations at the lower end of the R range, where the virial coefficient integrand is negligible, see below.

Figure 2 shows also that the interaction induced polarizability varies smoothly with the intermolecular geometry. Neglecting the shortest value of R ($R=2.75$ Å), with its own special features, as general behavior it is noted that the interaction induced polarizability is always positive for low values of θ ; it becomes negative at a value of θ which increases rapidly from $\theta \approx 45^\circ$ to $\theta \approx 60^\circ$ as R increases; it remains negative until the region around $\theta \approx 110$ – 120° (thus being negative around the T-shaped configurations (where the potential minimum is included) at θ close to 90°). At θ around 180° the interaction induced electric dipole polarizability starts as negative for small values of R and it becomes positive between $R=4.0$ Å and $R=4.5$ Å.

The integrands $I[\Delta\alpha]$, $I[\Delta\mu^2]$ and $I[\Delta\mu]$ for three temperatures (100 K, 298.15 K and 600 K) are shown in Fig. 3. They are plotted as a function of R at angles θ varying from 0 to 360 degrees in steps of 5 degrees. As expected, the integrands corresponding to the orientational contributions decrease rapidly in magnitude when the temperature increases. Those in the induction contribution go down at a considerably slower rate with the temperature. Note that $I[\Delta\alpha]$ and $I[\Delta\mu]$ show a similar profile, when the curves are mirrored through the x axis, whereas $I[\Delta\mu^2]$ is positive for all values of θ , and it appears to be of shorter range with respect to the other two integrands.

The semi-classical integrals $X[T, r, I[\Delta\alpha]]$ (defined in Eq. 1), $X[T, r, I[\Delta\mu^2]]$ (Eq. 8)

and $X[T, r, I[\Delta\mu]]$ (Eq. 9) were computed employing two different and independent approaches, both with MATHEMATICA: by employing the NINTEGRATE internal routine performing directly the two-dimensional integration, *and* by splitting the two-dimensional integrals in two parts, first integrating for each of 180 different values of θ the corresponding function of R on the R variable, with a numerical procedure in a grid of 600 values of R between the limits of integration, and then integrating numerically on θ . The dependence on the limits of integrations has been carefully monitored. In all cases the results did not change appreciably when the lower integration limit (R_{min}) was gradually lowered from $R_{min}=3.21 \text{ \AA}$ (1.7 au) to 2.46 \AA (1.3 au). The data shown below correspond the choice $R_{min}=2.46 \text{ \AA}$. A variety of choices for the higher integration limit (R_{max}) were tested. In the two-step integration $R_{max}=320 \text{ \AA}$ in all cases. In the direct two-dimensional integration $R_{max}=80 \text{ \AA}$ for $X[T, r, I[\Delta\alpha]]$, whereas for $X[T, r, I[\Delta\mu^2]]$ and $X[T, r, I[\Delta\mu]]$ we have monitored the convergence of the results by performing integrations at values of R_{max} increasing from $R_{max}=20 \text{ \AA}$ to $R_{max}=320 \text{ \AA}$. As it could also be inferred from Fig. 3, convergence in the case of $X[T, r, I[\Delta\mu^2]]$ was very rapid. Conversely, the integrand in $X[T, r, I[\Delta\mu]]$ decays at a slower pace at long range. In this case the integrals obtained at increasing higher integration limits were fitted to a polynomial in R_{max}^{-1} , keeping as final value the $R_{max} \rightarrow \infty$ extrapolation. All in all, the values obtained with the two integration procedures describe above were very close, with differences lower than the number of digits given in the Tables below.

The conversion factors used for B_ϵ are $1 \text{ au} = a_0^6 \text{ mol}^{-2} = 2.19587 \times 10^{-50} \text{ cm}^6 \text{ mol}^{-2}$.

III. THE VIRIAL COEFFICIENTS

The results for the CO-Ar dielectric second virial coefficients in the range of temperatures from 140 to 600 K are given in Table IV and plotted in Fig. 4. The individual contributions are also included. The behavior of the dielectric coefficient with the temperature is different from that found for diatomic rare gas van der Waals complexes, see Ref. 25 where $B_\epsilon(T)$ always decreased with an increased temperature. Here we have a clear increase in the dielectric coefficient with the temperature. As expected, for large temperatures the dominating contribution is given by $B_\epsilon(\text{ind})$. For each temperature $B_\epsilon^{(\Delta\mu)}$ (or) is about twice $B_\epsilon^{(\Delta\mu^2)}$ (or) and of opposite sign. The combination of the two ori-

entational contributions therefore yields a partial cancellation, thus giving rise to a smaller orientational contribution to the property compared to the electronic effect included in $B_\epsilon(\text{ind})$. For low temperatures the orientational contribution is larger in absolute value and plays a role in modulating the dependence of the property with the temperature. Around room temperature, we estimate a second dielectric virial coefficient of the CO-Ar van der Waals complex of $\approx 1.9 \text{ cm}^6 \text{ mol}^{-1}$.

Considering the accuracy of our previous theoretical calculations,²⁻⁴ it is reasonable to claim that the present results are predictive and that they may serve as benchmarks for additional theoretical and experimental investigations on CO-Ar.

To give an idea of the quality of the interaction potential $\Delta V(r, R, \theta)$ employed in the semiclassical determination of the dielectric second virial coefficients of the CO-Ar van der Waals complex, and as a natural extension of the analysis, the pressure second virial coefficient was also evaluated according to³⁵

$$B(T) = N_A \pi \int \left[1 - \exp\left(-\frac{\Delta V(r, R, \theta)}{kT}\right) \right] R^2 dR \sin \theta d\theta = \frac{N_A}{2} X[T, r, I[g]]. \quad (15)$$

The results yielded by the CCSD(T)/aug-cc-pVQZ-33211 surface from Ref. 2 are compared to those obtained in this work by employing the CCSD(T)/aug-cc-pVTZ-33221 potential taken from Ref. 36.

The integrands $I[g]$ appearing in $B(T)$ show a peculiar behavior with respect to the temperature (see Fig. 5, where $I[g]$ is shown for the potential of Ref. 2). At low temperature and intermediate values of θ the negative part of the integrand clearly dominates. As the temperature increases the negative and positive reach about the same magnitude, cancelling out almost exactly at around 375 K, where the virial coefficient $B(T)$ vanishes. At larger temperatures the positive contribution slightly dominates.

The integration in $X[T, r, I[g]]$ is carried out in the range $R_{\min}=1.27 \text{ \AA}$ to $R_{\max}=200 \text{ \AA}$. The functional form given in Ref. 2 yields somewhat inaccurate potential energy values below the chosen R_{\min} . Since the integrand is still quite sizable at such low distance, see Figure 5, values of the integrals at a few (five) values of R_{\min} (starting from 1.3 \AA and increasing) were computed, for each T . A cubic fit was performed for these five values as a function of R_{\min} , and a limit for $R_{\min} \rightarrow 0$ was performed. Good accuracy was achieved only when we performed the two-step integration described above, where the two-dimensional integrals are split in two parts, first integrating on the R variable, for

1
2
3 each of 180 different values of θ , the corresponding function of R , computed numerically
4 this time on a finer grid of 4000 values of R between R_{min} and 320 Å. Then the integration
5 on θ was performed.
6
7

8
9 In Fig. 6 we report the CO-Ar theoretical pressure second virial coefficients, obtained
10 with the potentials in Refs. 2 and 36. The differences between the two sets of values are
11 very small and larger at low temperatures. The values obtained from the potential in
12 Ref. 36 are always lower than those calculated from the other potential. In Fig. 6 we
13 also compare our results with the available experimental data^{37,38} and with the results of
14 *ab initio* calculations by Gianturco and co-workers.³⁹ Except for the lowest temperature,
15 the theoretical results are within the experimental error bars.
16
17
18
19
20
21
22
23
24
25
26
27
28
29
30
31
32
33
34
35
36
37
38
39
40
41
42
43
44
45
46
47
48
49
50
51
52
53
54
55
56
57
58
59
60

IV. CONCLUDING REMARKS

Using the CCSD(T)/aug-cc-pVQZ-33211 intermolecular potential energy surface from Ref. 2, the CCSD aug-cc-pVTZ-33211 interaction induced dipole moment surface from Ref. 3, and the CCSD/d-aug-cc-pVTZ-33211 interaction induced polarizability surface calculated in the present work, we have evaluated the CO-Ar pressure and dielectric second virial coefficients. While excellent agreement between theoretical and experimental pressure coefficients is obtained, no previous experimental or theoretical investigations have been reported on the dielectric second virial coefficient. We do expect, however, that the present results, estimating a second dielectric virial coefficient of the CO-Ar van der Waals complex of $\approx 1.9 \text{ cm}^6 \text{ mol}^{-1}$ around room temperature, are predictive and may be used as benchmarks for future studies of the CO-Ar van der Waals complex.

The dielectric second virial coefficient of the CO-Ar complex results from a partial cancellation between the two combined orientational contributions (which show a quite pronounced temperature dependence and are of opposite sign) and a weakly temperature dependent electronic contribution. Work is under way in our group to compute the frequency dispersion of the collision induced electric dipole polarizability, along the lines of the procedure adopted in our studies of the noble gas van der Waals dimers.^{16–18,21,23–25} This can be used to compute the refractivity second virial coefficient,⁴⁰ which accounts only for the effect of the electronic induced moment effect – the orientational contributions averaging to zero in the dynamic regime – besides being, together with the static induced electric dipole polarizability studied here, an essential ingredient also for studies of the second Kerr virial coefficient^{41,42} and of the collisional induced scattering of light (CILS).^{43,44}

Acknowledgements

This work has been supported by the European Research and Training Network NANOQUANT, contract No. MRTN-CT-2003-506842, and by the Spanish Ministerio de Educación y Ciencia and FEDER (CTQ2005-01076 project).

For Peer Review Only

Figure Captions

Figure 1 The interaction induced electric dipole moment as a function of the angle θ for a choice of values of R . Comparison of computed (symbols) and interpolated (full curves) values. Both the x and z components are shown.

Figure 2 The interaction induced electric dipole polarizability as a function of the angle θ for a choice of values of R . Comparison of computed (symbols) and interpolated (full curves) values. The top panel is devoted to the shorter range, R between 2.75 and 5.0 Å. The lower panel shows the longer range, with R between 6.0 and 20.0 Å.

Figure 3 The integrands $I[\Delta\alpha]$ (appearing in $B_\epsilon(\text{ind})$), $I[\Delta\mu^2]$ (appearing in $B_\epsilon^{(\Delta\mu^2)}(\text{or})$) and $I[\Delta\mu]$ (appearing in $B_\epsilon^{(\Delta\mu)}(\text{or})$) as a function of R and θ for three temperatures $T=100$ K, $T=298.15$ K and $T=600$ K.

Figure 4 The dielectric second virial coefficients.

Figure 5 The integrand $I[g]$ appearing in $B(T)$, the pressure virial coefficient, shown as a function of R and θ for three temperatures $T=100$ K, $T=298.15$ K and $T=600$ K.

Figure 6 The pressure virial coefficients.

-
- 1
2
3
4
5
6
7
8
9
10
11
12
13
14
15
16
17
18
19
20
21
22
23
24
25
26
27
28
29
30
31
32
33
34
35
36
37
38
39
40
41
42
43
44
45
46
47
48
49
50
51
52
53
54
55
56
57
58
59
60
- ¹ HAVENITH, M. and SCHWAAB, G. W., *Z. Phys. Chem.* **219**, 1053 (2005).
 - ² PEDERSEN, T. B., CACHEIRO, J. L., B. FERNÁNDEZ and KOCH, H., *J. Chem. Phys.* **117**, 6562 (2002).
 - ³ CACHEIRO, J. L., B. FERNÁNDEZ, PEDERSEN, T. B. and KOCH, H., *J. Chem. Phys.* **118**, 9596 (2003).
 - ⁴ MANTZ, A. W., THIBAUT, F., CACHEIRO, J. L., B. FERNÁNDEZ, PEDERSEN, T. B., KOCH, H., VALENTIN, A., CLAVEAU, C., HENRY, A., and HURTMANS, D., *J. Mol. Spectrosc.* **222**, 131 (2003).
 - ⁵ PURVIS, G. D. and BARTLETT, R. J., *J. Chem. Phys.* **76**, 1910 (1982).
 - ⁶ RAGHAVACHARI, K., TRUCKS, G. W., POPLE, J. A. and HEAD-GORDON, M., *Chem. Phys. Lett.* **157**, 479 (1989).
 - ⁷ KENDALL, R. A., T. H. DUNNING, JR. and HARRISON, R. J., *J. Chem. Phys.* **96**, 6796 (1992).
 - ⁸ WOON, D. E. and T. H. DUNNING, JR., *J. Chem. Phys.* **98**, 1358 (1993).
 - ⁹ KOCH, H., FERNÁNDEZ, B. and CHRISTIANSEN, O., *J. Chem. Phys.* **108**, 2784 (1998).
 - ¹⁰ STONE, A. J. *The Theory of Intermolecular Forces*. Oxford University Press, Oxford, 1996.
 - ¹¹ BUCKINGHAM, A. D. and RAAB, R. E., *Trans. Faraday Soc.* **54**, 623 (1958).
 - ¹² MOLDOVER, M. R., *J. Res. Natl. Inst. Stand. Technol.* **103**, 167 (1998).
 - ¹³ MOLDOVER, M. R., *J. Res. Natl. Inst. Stand. Technol.* **105**, 667 (2000).
 - ¹⁴ MOLDOVER, M. R. and BUCKLEY, T. J., *Int. J. Thermophysics.* **22**, 859 (2001).
 - ¹⁵ MOSZYNSKI, R., Theory of Intermolecular Forces: an Introductory Account, in *Molecular Materials with Specific Interactions Modeling and Design*, edited by PAPADOPOULOS, M. G., SADLEJ, A. J. and LESZCZYNSKI, J., volume 4 of *Challenges and Advances in Computational Chemistry and Physics*. Springer, 2007.
 - ¹⁶ FERNÁNDEZ, B., HÄTTIG, C., KOCH, H. and RIZZO, A., *J. Chem. Phys.* **110**, 2872 (1999).
 - ¹⁷ HÄTTIG, C., LARSEN, H., OLSEN, J., JØRGENSEN, P., KOCH, H., FERNÁNDEZ, B. and RIZZO, A., *J. Chem. Phys.* **111**, 10099 (1999).
 - ¹⁸ KOCH, H., HÄTTIG, C., LARSEN, H., OLSEN, J., JØRGENSEN, P., FERNÁNDEZ, B. and RIZZO, A., *J. Chem. Phys.* **111**, 10108 (1999).

- 1
2
3 19 RIZZO, A., RUUD, K. and BISHOP, D. M., *Mol. Phys.* **100**, 799 (2002).
4
5 20 PECUL, M. and RIZZO, A., *Mol. Phys.* **100**, 447 (2002).
6
7 21 RIZZO, A., HÄTTIG, C., FERNÁNDEZ, B. and KOCH, H., *J. Chem. Phys.* **117**, 2609 (2002).
8
9 22 MARCHESAN, D., CORIANI, S. and RIZZO, A., *Mol. Phys.* **101**, 1851 (2003).
10
11 23 HÄTTIG, C., CACHEIRO, J. L., FERNÁNDEZ, B. and RIZZO, A., *Mol. Phys.* **101**, 1983
12 (2003).
13
14 24 CACHEIRO, J. L., FERNÁNDEZ, B., MARCHESAN, D., CORIANI, S., HÄTTIG, C. and RIZZO,
15 A., *Mol. Phys.* **102**, 101 (2004).
16
17 25 RIZZO, A., CORIANI, S., MARCHESAN, D., LÓPEZ CACHEIRO, J., FERNÁNDEZ, B. and
18 HÄTTIG, C., *Mol. Phys.* **104**, 305 (2006).
19
20 26 SUTTER, H. and COLE, R. H., *J. Chem. Phys.* **52**, 132 (1970).
21
22 27 BUCKINGHAM, A. D., COLE, R. H. and SUTTER, H., *J. Chem. Phys.* **52**, 5960 (1970).
23
24 28 COPELAND, T. G. and COLE, R. H., *J. Chem. Phys.* **64**, 1741 (1976).
25
26 29 BUCKINGHAM, A. D. and POPLE, J. A., *Trans. Faraday Soc.* **51**, 1179 (1955).
27
28 30 HUBER, K. and HERZBERG, G. *Molecular Spectra and Molecular Structure. IV. Constants*
29 *of Diatomic Molecules*. Van Nostrand Reinhold, New York, 1979.
30
31 31 To be published as supplementary material.
32
33 32 OGILVIE, J. F., CHEAH, S. L., LEE, Y. P. and SAUER, S. P. A., *Theor. Chem. Acc.* **108**,
34 85 (2002).
35
36 33 *DALTON*, a molecular electronic structure program, Release 2.0, 2005. See
37 <http://www.kjemi.uio.no/software/dalton/dalton.html>.
38
39 34 BOYS, S. F. and BERNARDI, F., *Mol. Phys.* **19**, 553 (1970).
40
41 35 HIRSCHFELDER, J. O., CURTISS, C. F. and BIRD, R. B. *Molecular Theory of Gases and*
42 *Liquids*. John Wiley and Sons, Inc., 1954.
43
44 36 TOCZYLOWSKI, R. R. and CYBULSKI, S. M., *J. Chem. Phys.* **112**, 4604 (2000).
45
46 37 DYMOND, J. H. and SMITH, E. B. *The Virial Coefficients of Pure Gases and Mixtures*.
47 Clarendon Press, Oxford, 1980.
48
49 38 BREWER, J. *AFOSR Report 67-2795 (Dec. 1967)*. Available from the Clearinghouse for
50 *Federal Scientific and Technical Information*, Doc. AD 663448.
51
52 39 GIANTURCO, F. A., PAESANI, F., LARANJEIRA, M. F., VASSILENKO, V. and CUNHA,
53 M. A., *J. Chem. Phys.* **110**, 7832 (1999).
54
55
56
57
58
59
60

- 1
2
3
4
5
6
7
8
9
10
11
12
13
14
15
16
17
18
19
20
21
22
23
24
25
26
27
28
29
30
31
32
33
34
35
36
37
38
39
40
41
42
43
44
45
46
47
48
49
50
51
52
53
54
55
56
57
58
59
60
- ⁴⁰ BUCKINGHAM, A. D. and POPLE, J., *Trans. Faraday Soc.* **51**, 1029 (1955).
- ⁴¹ BUCKINGHAM, A. D., *Proc. Roy. Soc. A.* **68**, 910 (1955).
- ⁴² COULING, V. W. and GRAHAM, C., *Mol. Phys.* **93**, 1 (1998).
- ⁴³ FROMMHOLD, L., *Adv. Chem. Phys.* **46**, 1 (1981).
- ⁴⁴ JOSLIN, C. G., GODDARD, J. D. and GOLDMAN, S., *Mol. Phys.* **89**, 7911 (1996).

For Peer Review Only

TABLE I: The parameters $C_{\lambda\rho}^{\sigma}$ and D_{ρ}^{σ} ($\sigma=x, z$) for the functional fit employed for the interaction dipole moment, see Eqs. 12 and 13.

	$\Delta\mu_x$	$\Delta\mu_z$		$\Delta\mu_x$	$\Delta\mu_z$
$C_{1,1}$	3.91465×10^5	1.87885×10^2	$C_{6,4}$	-1.23584×10^7	7.46147×10^6
$C_{1,2}$	-3.75769×10^5	-2.38171×10^4	$C_{6,5}$	1.12697×10^7	-1.47233×10^6
$C_{1,3}$	-3.43456×10^4	7.44944×10^4	$C_{7,1}$	1.00642×10^7	1.80247×10^4
$C_{1,4}$	1.54180×10^5	-6.24732×10^4	$C_{7,2}$	-9.62275×10^6	-1.55678×10^6
$C_{1,5}$	-1.37621×10^5	1.25015×10^4	$C_{7,3}$	-1.07151×10^6	4.67473×10^6
$C_{2,1}$	-3.32765×10^6	-9.94104×10^2	$C_{7,4}$	5.92065×10^6	-3.82642×10^6
$C_{2,2}$	3.18094×10^6	8.58094×10^4	$C_{7,5}$	-5.40084×10^6	7.56798×10^5
$C_{2,3}$	3.57644×10^5	-2.57635×10^5	$C_{8,1}$	-2.98082×10^6	-5.32695×10^3
$C_{2,4}$	-1.98406×10^6	2.10798×10^5	$C_{8,2}$	2.85038×10^6	4.59709×10^5
$C_{2,5}$	1.80931×10^6	-4.16360×10^4	$C_{8,3}$	3.15879×10^5	-1.38108×10^6
$C_{3,1}$	1.18704×10^7	7.91707×10^3	$C_{8,4}$	-1.74337×10^6	1.13151×10^6
$C_{3,2}$	-1.13441×10^7	-6.65128×10^5	$C_{8,5}$	1.59076×10^6	-2.24982×10^5
$C_{3,3}$	-1.29102×10^6	1.99037×10^6	$C_{9,1}$	4.91416×10^5	8.34426×10^2
$C_{3,4}$	7.23119×10^6	-1.62537×10^6	$C_{9,2}$	-4.69967×10^5	-7.22424×10^4
$C_{3,5}$	-6.59886×10^6	3.21020×10^5	$C_{9,3}$	-5.18174×10^4	2.17341×10^5
$C_{4,1}$	-2.34532×10^7	-2.49611×10^4	$C_{9,4}$	2.85563×10^5	-1.78395×10^5
$C_{4,2}$	2.24185×10^7	2.16785×10^6	$C_{9,5}$	-2.60628×10^5	3.57675×10^4
$C_{4,3}$	2.52486×10^6	-6.51462×10^6	$C_{10,1}$	-3.43205×10^4	
$C_{4,4}$	-1.40176×10^7	5.33351×10^6	$C_{10,2}$	3.28259×10^4	
$C_{4,5}$	1.27818×10^7	-1.05403×10^6	$C_{10,3}$	3.60245×10^3	
$C_{5,1}$	2.78265×10^7	3.94506×10^4	$C_{10,4}$	-1.98259×10^4	
$C_{5,2}$	-2.66018×10^7	-3.44090×10^6	$C_{10,5}$	1.80988×10^4	
$C_{5,3}$	-2.98086×10^6	1.03439×10^7	D_1	5.73841	5.02654
$C_{5,4}$	1.64883×10^7	-8.46936×10^6	D_2	5.72854	5.88734
$C_{5,5}$	-1.50322×10^7	1.67158×10^6	D_3	6.33533	6.13020
$C_{6,1}$	-2.09231×10^7	-3.49795×10^4	D_4	7.31722	6.35669
$C_{6,2}$	2.00036×10^7	3.03488×10^6	D_5	7.44852	7.03447
$C_{6,3}$	2.23549×10^6	-9.11657×10^6			

TABLE II: Counterpoise corrected CCSD/d-aug-cc-pVTZ-33211 interaction induced isotropic polarizability of CO-Ar in au. R is given in Å and θ in degrees.

θ/R	2.75	3.175	3.5	4.0	4.5	5.0	6.0	7.0	8.0	9.0	11.0	14.0	17.0	20.0
0	0.0763808	0.0866994	0.1345057	0.1476057	0.1197253	0.0882244	0.0476887	0.0284033	0.0184480	0.0126149	0.0066617	0.0031446	0.0017283	0.0010498
30	0.0386546	0.0392243	0.0821976	0.0983557	0.0802062	0.0582864	0.0304354	0.0177531	0.0113922	0.0077538	0.0040610	0.0019145	0.0010537	0.0006412
60	-0.3223836	-0.1506960	-0.0635973	-0.0090560	0.0011397	0.0002646	-0.0023889	-0.0024526	-0.0019292	-0.0014843	-0.0008978	-0.0004409	-0.0002431	-0.0001470
90	-0.4484664	-0.2231380	-0.1176435	-0.0456437	-0.0246910	-0.0187517	-0.0137206	-0.0097813	-0.0069328	-0.0050440	-0.0028845	-0.0014240	-0.0007998	-0.0004924
120	0.0843583	-0.0363191	-0.0109907	0.0247243	0.0287074	0.0205706	0.0070567	0.0021501	0.0006217	0.0000521	-0.0002346	-0.0001951	-0.0001311	-0.0000888
150	0.7307725	-0.0483683	-0.0724280	0.0172912	0.0562743	0.0537627	0.0298857	0.0165756	0.0103367	0.0069739	0.0036579	0.0017464	0.0009742	0.0005992
180	0.5699465	-0.3413510	-0.2700327	-0.0594017	0.0366547	0.0540303	0.0356417	0.0211159	0.0137463	0.0095738	0.0052627	0.0026001	0.0014761	0.0009178

TABLE III: Parameters of the analytic surface, Eq. 14 used to fit the interaction induced isotropic polarizability calculated at the CCSD/d-aug-cc-pVTZ-33211 level.

Parameter		Parameter	
C ₀₀	235.982524	C ₄₀	23.242990
C ₀₁	117.013050	C ₄₁	4.211370
C ₀₂	70.051774	C ₄₂	-5.860846
C ₀₃	62.176476	C ₄₃	1.504238
C ₀₄	27.983865	C ₄₄	-0.176698
C ₀₅	-25.984205	C ₄₅	0.010477
C ₀₆	8.327798	C ₄₆	-0.000266
C ₁₀	-116.141705	C ₅₀	0.435423
C ₁₁	-32.827401	C ₅₁	5.052074
C ₁₂	45.578439	C ₅₂	-9.953601
C ₁₃	-14.181304	C ₅₃	3.582890
C ₁₄	2.107401	C ₅₄	-0.694699
C ₁₅	-0.155488	C ₅₅	0.085258
C ₁₆	0.004632	C ₅₆	-0.005429
C ₂₀	35.402619	C ₆₀	-1.597688
C ₂₁	128.527546	C ₆₁	1.762004
C ₂₂	-89.918426	C ₆₂	-0.623128
C ₂₃	24.492478	C ₆₃	0.100749
C ₂₄	-3.407260	C ₆₄	-0.007654
C ₂₅	0.240823	C ₆₅	0.000229
C ₂₆	-0.006973	C ₆₆	0.000000
C ₃₀	-91.951356	D ₀	2.701917
C ₃₁	4.440155	D ₁	0.886300
C ₃₂	15.318405	D ₂	0.891755
C ₃₃	-5.227270	D ₃	0.879037
C ₃₄	0.772246	D ₄	0.891510
C ₃₅	-0.056269	D ₅	1.608195
C ₃₆	0.001689	D ₆	1.123331

TABLE IV: CO-Ar dielectric second virial coefficients in cm^6/mol .

T/K	$B_\epsilon(\text{ind})$	$B_\epsilon^{(\Delta\mu^2)}(\text{or})$	$B_\epsilon^{(\Delta\mu)}(\text{or})$	$B_\epsilon(T)$
140	3.771	4.066	-6.618	1.219
160	3.723	3.355	-5.924	1.154
180	3.683	2.865	-5.332	1.216
200	3.649	2.508	-4.837	1.320
220	3.619	2.237	-4.418	1.438
240	3.592	2.025	-4.061	1.556
260	3.568	1.855	-3.754	1.669
280	3.546	1.715	-3.488	1.773
300	3.526	1.598	-3.256	1.869
320	3.509	1.500	-3.050	1.959
340	3.490	1.415	-2.867	2.037
360	3.473	1.341	-2.704	2.110
380	3.457	1.277	-2.558	2.176
400	3.442	1.220	-2.426	2.237
420	3.428	1.170	-2.306	2.292
440	3.415	1.124	-2.197	2.342
460	3.401	1.084	-2.097	2.388
480	3.389	1.047	-2.005	2.431
500	3.377	1.013	-1.920	2.470
520	3.365	0.983	-1.842	2.506
540	3.353	0.955	-1.769	2.539
560	3.342	0.929	-1.702	2.569
580	3.331	0.905	-1.639	2.597
600	3.321	0.883	-1.580	2.624

Figure 1 - Cacheiro et al., Mol. Phys.

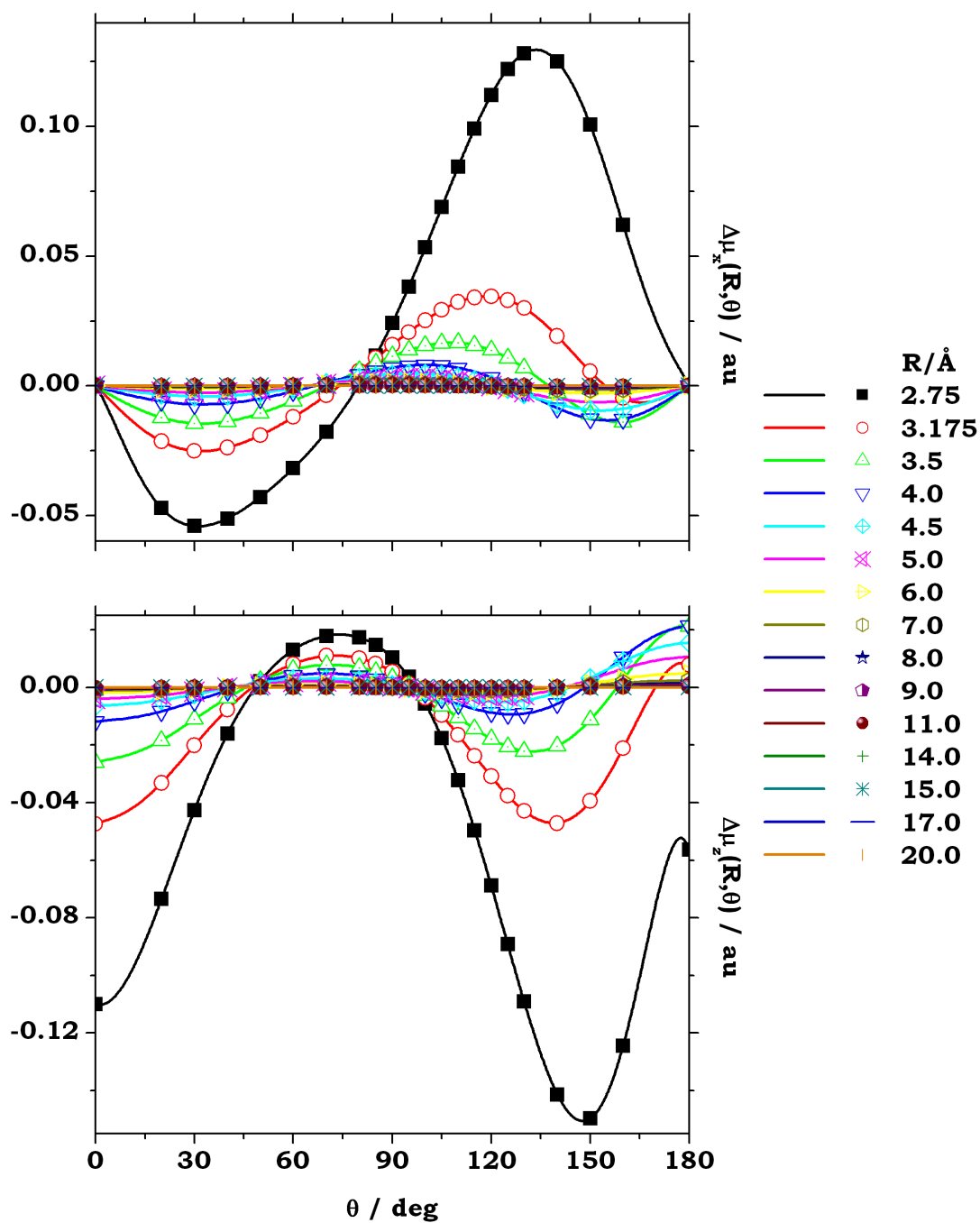


Figure 2 - Cacheiro et al., Mol. Phys.

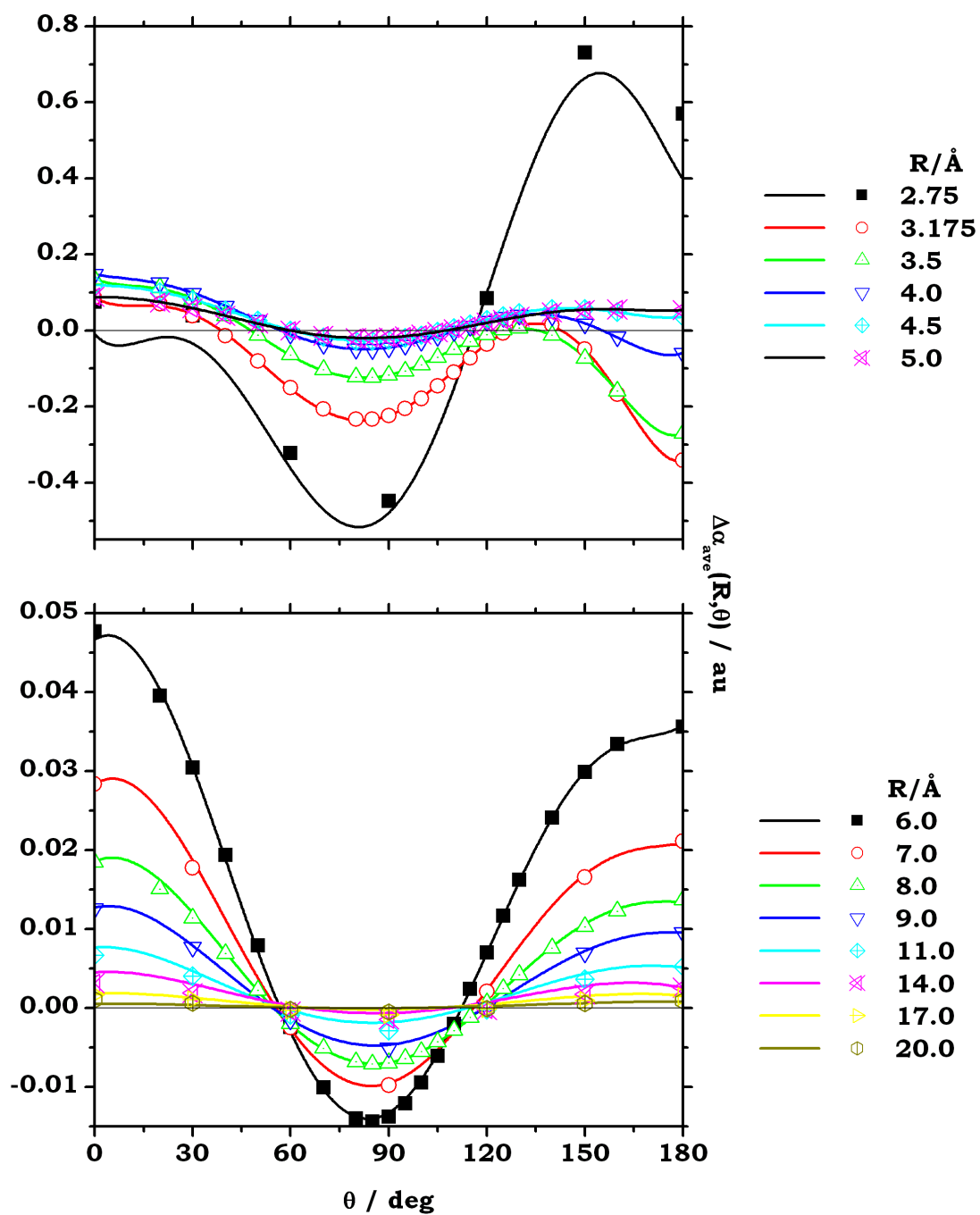


Figure 3 - Cacheiro et al., Mol. Phys.

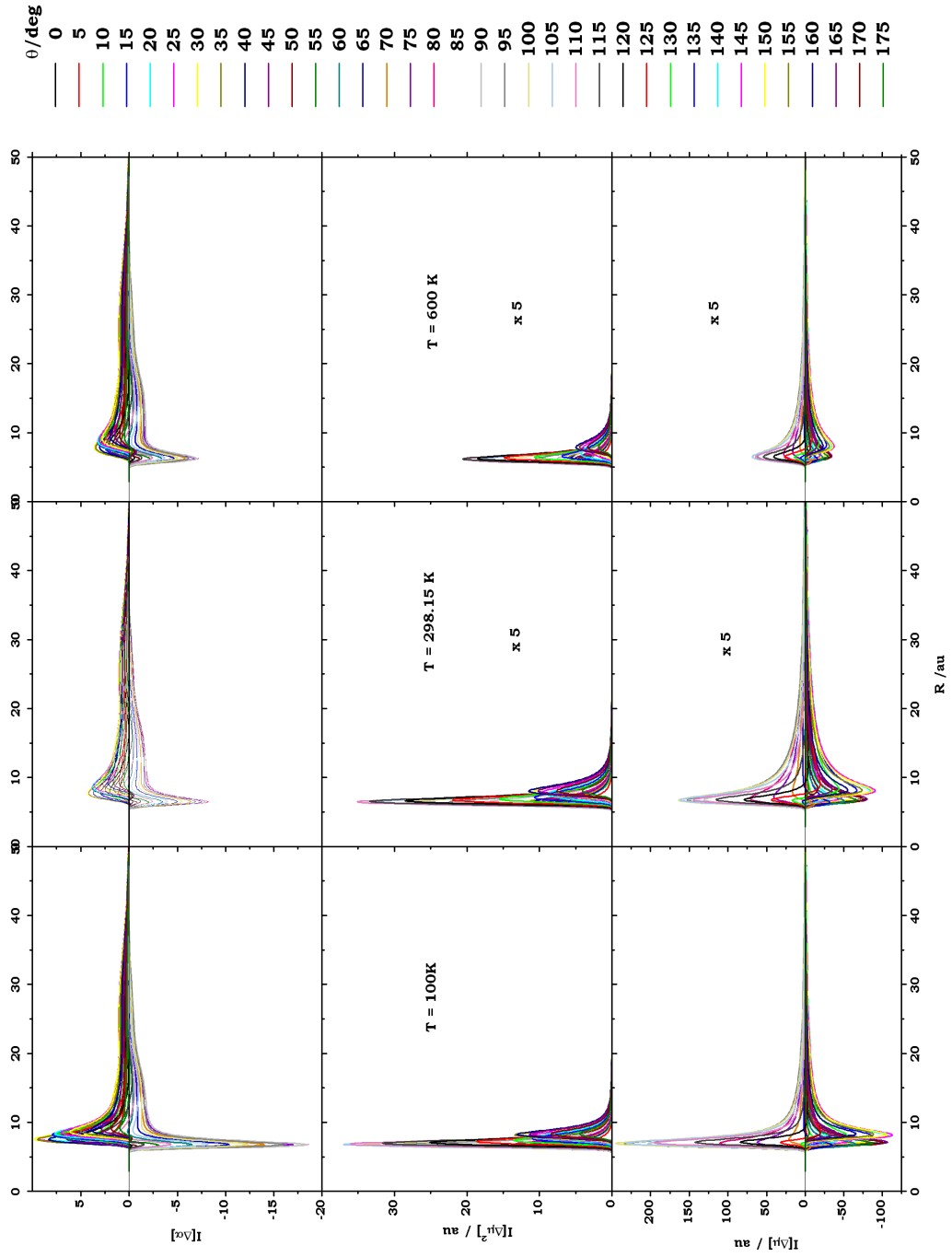


Figure 4 - Cacheiro et al., Mol. Phys.

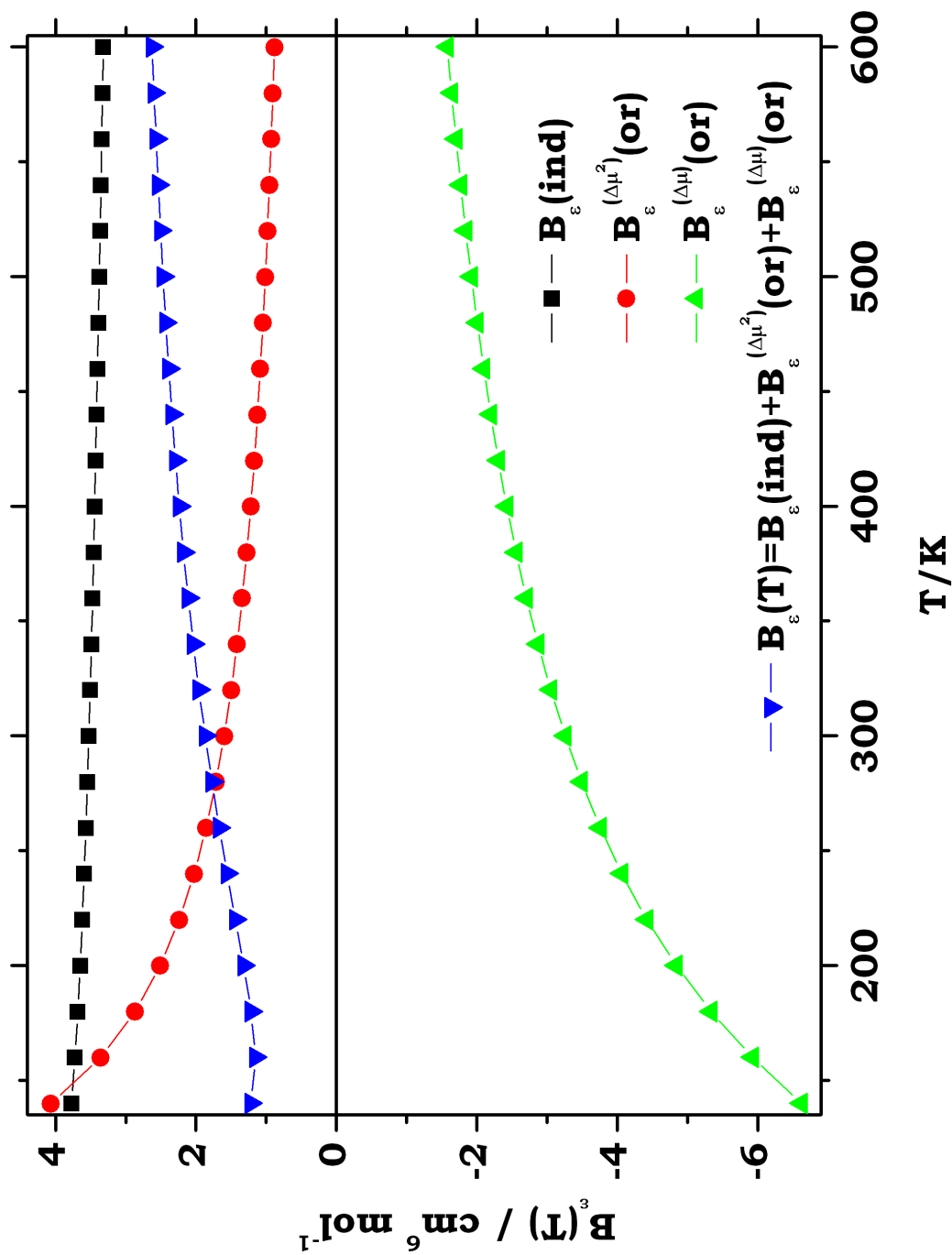


Figure 5 - Cacheiro et al., Mol. Phys.

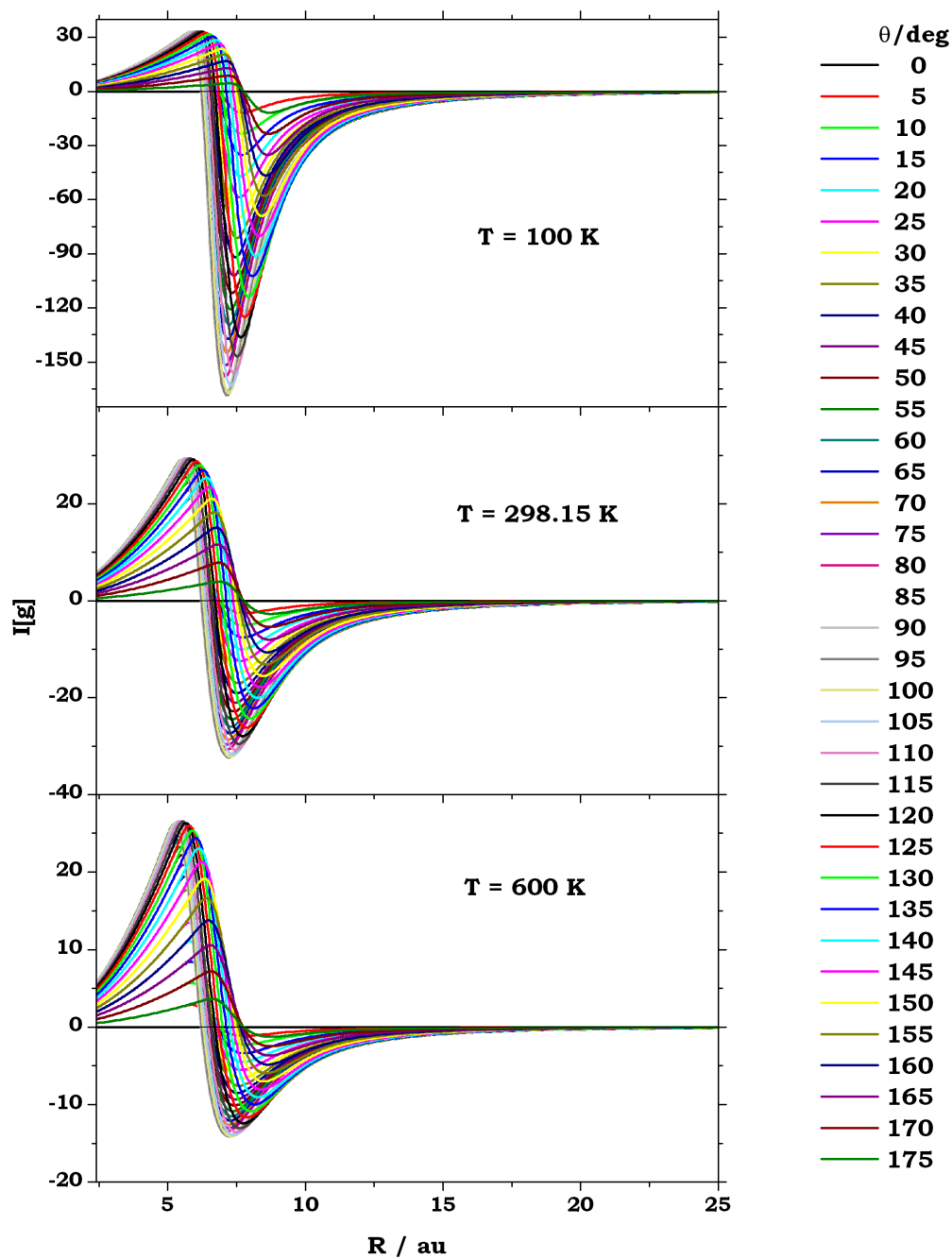


Figure 6 - Cacheiro et al., Mol. Phys.

